Electrochimica Acta 467 (2023) 143120

Contents lists available at ScienceDirect

Electrochimica Acta

journal homepage: www.journals.elsevier.com/electrochimica-acta

Behavior of a forest of NiFe nanowires in KOH and NaCl solution for water electrolysis

S. Carbone [a], F. Proietto [a], F. Bonafede [a], R.L. Oliveri [a], B. Patella [a], F. Ganci [a,b], G. Aiello [a], P. Mandin [c], M. Kim [d], M. Scopelliti [e,f], R. Inguanta [a,*]

[a] Dipartimento di Ingegneria, Università degli Studi di Palermo, Viale delle Scienze, Palermo 90128, Italy
[b] Corpo Nazione dei Vigili del Fuoco, Rome, Italy
[c] Institut de Recherche Dupuy de Lôme, UMR CNRS 6027, Lorient 56100, France
[d] Ocean and Mechanical Engineering, Florida Atlantic University, 777 Glades Rd., Boca Raton, FL 33431, USA
[e] Dipartimento di Fisica e Chimica - Emilio Segrè, Università degli Studi di Palermo, Viale delle Scienze 17, Palermo 90128, Italy
[f] Laboratorio Superfici, Film Sottili e Dispositivi, ATeN Center, Università degli Studi di Palermo, Viale delle Scienze 18/A, Palermo 90128, Italy

ARTICLE INFO

Keywords:
Nanostructured electrode
Nanowires
NiFe alloy
Alkaline electrolyzers
Template electrosynthesis
Seawater electrolysis

ABSTRACT

The present work investigates the behavior of nanostructured electrodes consisting of an array of nanowires of NiFe alloy in KOH + 0.5 M NaCl solution. The aim is to explore the possibility of using these electrodes for hydrogen production by seawater electrolysis. Seawater splitting requires a highly selective electrode on the anode side, where the evolution of molecular chlorine or the formation of other active chlorine compounds can compete with the oxygen evolution reaction. Nanostructured electrodes, obtained by template electrosynthesis, were tested at room temperature in KOH + 0.5 M NaCl solution, and the results were compared with those obtained in pure KOH. The results showed that the presence of NaCl does not affect the electrocatalytic behavior of the nanostructured NiFe alloy. Furthermore, the chemical–physical characterizations carried out after the long-term galvanostatic tests, have shown that the nanostructured electrodes are also stable in terms of morphology and composition. In addition, the solution used to perform the long-term galvanostatic tests was analyzed to investigate the possible formation of chlorine compounds. The absence of these compounds, together with the measured potential value measured for the oxygen evolution reaction, which was always lower than the thermodynamic redox potential for the hypochlorite formation reaction, leads us to conclude that these electrodes are potentially suitable for seawater electrolysis.

1. Introduction

The use of renewable energy sources for electricity generation is the only way to reduce greenhouse gas emissions [1,2]. Due to the unpredictability of these sources, it is necessary to match them with energy storage systems, that help to maintain grid stability and increase efficiency [3,4]. Green hydrogen is undoubtedly suitable for energy storage, either for stand-alone or large-scale systems [5,6]. Today, green hydrogen is still not economically competitive as an energy carrier due to the high materials and electricity costs required for its production [7,8]. Hydrogen production costs can be reduced by increasing the low-cost renewable electricity production, increasing the power output of renewable energy sources, and increasing the efficiency of electrolyzers by using high-performance materials [9]. Using materials with high active surface areas may also contribute to the improved efficiency of the electrolyzers [10–15]. Nanostructured electrodes demonstrate exceptional electrocatalytic properties, as shown by extensive research carried out on other electrochemical devices [16] such as batteries [17–19], supercapacitors [20–23], sensors [24,25], fuel cells [26,27] and solar cells [28]. The unique properties of nanomaterials [29,30] are due to their high area-to-volume ratio, which is orders of magnitude higher than the geometric ratio, resulting in a very large number of catalytic sites available for reactions [31–34]. As reported by Darband et al. [35], the morphology of nanostructure leads to reduced reaction potential. This is due to the super aero-phobic surface of nanowires (NWs), which enables fast separation of gas bubbles from the surface [36] increasing the availability of free active sites [37]. Nanostructured electrodes achieve excellent performance, assisting in reducing

* Corresponding author.
E-mail address: rosalinda.inguanta@unipa.it (R. Inguanta).

https://doi.org/10.1016/j.electacta.2023.143120
Received 13 May 2023; Received in revised form 28 August 2023; Accepted 29 August 2023
Available online 1 September 2023

electrocatalyst mass, and consequently decreasing device weight and cost [38].

For application in water electrolysis, various nanomaterials such as oxides and alloys of precious and non-precious metals [39–41] have been studied for both the hydrogen evolution reaction (HER) [42–44] and the oxygen evolution reaction (OER) [45,46]. In particular, NiFe alloys are considered to be attractive low-cost electrocatalysts for promoting both HER and OER [47–52]. Zhu et al. [53] used nickel–iron hydroxide nanosheets electrodeposited on sintered stainless steel felt as a bifunctional electrocatalyst achieving an overall cell voltage of 1.80 V at 100 mA cm^{-2}. The NiFe-layered double hydroxide catalyst requires only 1.46 V to drive an electrolyzer at 10 mA cm^{-2} [54]. Other interesting results were obtained by Cheng et al. [55] and by Tang et al. [56] using different types of NiFe-based composite electrocatalysts.

NiFe-based electrocatalysts are also attractive for seawater electrolysis, as demonstrated by Duan et al. [57], who developed NiFe hydroxide nanosheets with high stability. Recently, Jiang et al. [58] have proposed NiFe layered double hydroxide nanosheets as electrocatalysts for overall seawater splitting. They found in alkaline simulated seawater (1.0 M KOH + 0.5 M NaCl) a low cell voltage of 1.55 V at 10 mA·cm^{-2} and long-term operational stability for 105 h at 100 mA cm^{-2}. These results are interesting since an obstacle to green hydrogen production is the use of deionized water, which is necessary to avoid catalyst poisoning and competitive reactions [59–61]. Freshwater resources are limited and the United Nations estimates that about one-third of the world's population lives in water-stressed areas [62]. Developing high-efficiency catalysts with high selectivity and stability is critical for seawater electrolysis to avoid the effects of various cations and anions present in natural seawater [63,64]. A challenge in seawater splitting is the high concentration of chloride anions (≈ 0.5 M in seawater) [65,66]. Therefore, seawater splitting requires highly selective electrodes, especially for the anodic side. In particular, chlorine evolution reaction (at lower pH) and hypochlorite formation (at higher pH) could be involved and compete with OER [67,68]. In addition, electrodes need to be robust against chloride corrosion [69,70]. For seawater electrolysis, the alkaline environment is the preferred one since it provides higher selectivity for OER and allows the use of non-noble metal catalysts. Additionally, alkaline electrolyzers are the most commercially available and established technologies [70]. However, the process of alkalinizing seawater involves the precipitation of Ca and Mg hydroxide, which may lead to fouling of the electrodes and consequently, performance loss. This limitation can be easily overcome by the process of decantation and filtration, resulting in a clear solution that is suitable for electrolysis [70].

In this work, we present the behavior of a mechanically stable forest of NiFe alloy nanowires. The distinctive characteristics of 1D nanomaterials, such as their high specific surface area and higher edge-to-face ratio, enhanced the electrochemical performance of the NiFe alloy [31,46]. Indeed, the high surface-to-volume ratio of nanostructures provides large electrochemical surface areas with a high number of active sites directly accessible to the electrolyte, guaranteeing better performance per unit of electrode area and/or mass of the material. Additionally, carrier transport paths are faster and shorter in a nanostructured electrode, facilitating the kinetics of the electrochemical reaction. NiFe NWs were obtained with a simple and above all reproducible and easily scalable method. Based on the results obtained in [46] where NiFe nanostructured electrodes were optimized and tested in a KOH solution, in this work the behavior in KOH + 0.5 M NaCl for both HER and OER was investigated. Specifically, the alloy with an optimized composition of about 79% Fe was tested to investigate the potential of employing these electrodes as bifunctional catalysts in seawater electrolysis. Various electrochemical tests were carried out at room temperature, and long-term galvanostatic tests (at ±50 mA cm^{-2} for 125 h) were also performed to study the stability of the electrodes. The results obtained were compared to those obtained in 30% KOH solution. The electrodes were characterized by different characterization techniques before and after the long-term galvanostatic tests to assess any changes in morphology and composition.

2. Materials and methods

NiFe NWs electrodes were prepared by template electrosynthesis, using a polycarbonate membrane as a template. The fabrication method is detailed in our previous work [46]. Briefly, a thin gold film was sputtered on one side of the template. Subsequently, on the gold side, nickel was electrodeposited to obtain a current collector, using a Watt's bath (300 g/L $NiSO_4 \cdot 6\ H_2O$, 45 g/L $NiCl_2$, 45 g/L H_3BO_3), by potentiostatic electrodeposition at −1.5 V vs. Saturated Calomel Electrode (SCE) for 1.5 h For the NWs deposition, following the results obtained in the previous work [46], a Watt's bath with 0.44 M $FeSO_4 \bullet 7\ H_2O$ was used. This bath (containing about 67% Ni and 33% Fe) was chosen because it led to the deposition of NiFe alloy NWs with the best performance corresponding to a composition of 21% Ni and 79% Fe. As reported in [46], this composition was confirmed using two different techniques, energy dispersive spectroscopy (EDS) and inductively coupled plasma optical emission spectrometry. NWs were obtained by pulse electrodeposition switching the potential between −1.35 (for 6 s) and −0.65 (for 4 s) V vs. SCE for 100 cycles (in Fig. S1 some cycles were reported). During the pulse at −1.35 V, a cathodic current density of about −8.5 mA cm^{-2} was measured. Instead, during the pulse at −0.65 V, an anodic current density in the range from 1.5 to 0.26 mA cm^{-2} was reached. As detailed in [71], the inversion of current density polarity allows for control of the nanostructure composition and the morphology. The electrodeposition was carried out in a standard three-electrode cell at room temperature. A Pt mesh was used as a counter electrode and a SCE as a reference. After electrodeposition, the samples were etched in pure $CHCl_3$ to remove the polycarbonate template. The load of NiFe NWs on the Ni current collector was evaluated by gravimetric measurements using a Sartorius microbalance (Premium Microbalance ME36S). We have measured a specific load, with respect to the geometrical area of the electrode, of about 3.31(±3.87%) mg/cm^2.

Electrochemical characterizations were carried out in a 30% w/w KOH aqueous solution with 0.5 M NaCl (from here KOH+NaCl) and for comparison also in 30% KOH aqueous solution (from here KOH). A Ni sheet was used as a counter-electrode, and Hg/HgO 0.1 M NaOH was used as a reference. In the following, all the potentials will be referred to the value of the Reversible Hydrogen electrode (RHE) at pH 14. All the tests were performed at room temperature and without stirring. Quasi-steady-state polarization (QSSP), cyclovoltammetry (CV), and galvanostatic-step polarization were performed. In addition, galvanostatic tests at ±50 mA cm^{-2} were carried out to study the mid- and long-term behavior of electrodes. All the tests were performed both for HER and OER. A multichannel Cell Test System (Solartron, Mod. 1470 E) was used to perform the electrochemical characterization, and the data were recorded by MultiStat Software. Each experiment was repeated at least three times.

The NWs-based electrodes were characterized before and after the long-term galvanostatic tests by scanning electron microscopy (SEM) using a FEG-ESEM microscope (QUANTA 200 by FEI), and EDS to evaluate the NWs morphology and composition. In addition, NWs electrodes were characterized by X-ray diffraction (XRD) using a RIGAKU X-ray diffractometer (D-MAX 25,600 HK) in the 2θ range from 3° to 100°. The surface of the NWs used to perform the OER long-term galvanostatic tests was also characterized by means of X-ray photoelectron spectroscopy (XPS) using a PHI5000 VersaProbe II (ULVAC-PHI), working with an Al anode (Al K_α = 1486.6 eV), using a 200 μm ⌀ beam (50 W) and collecting electrons taking off at 45° from the surface while neutralizing charges with both electrons and ions guns. Survey (Pass Energy, PE = 117.400 eV; resolution 1.0 eV) and high-resolution spectra (PE = 29.350 eV; resolution 0.05 eV), in the Ni $2p_{3/2}$, Fe $2p_{3/2}$ and C 1s regions, were collected for NiFe samples before and after the

long-term tests in KOH+NaCl solution.

The solution used to perform the long-term galvanostatic tests was analyzed to investigate the possible formation of chlorine compounds. The presence of hypochlorite (ClO^-) and hypochlorous acid (HClO) was checked using an Agilent Cary 60 UV spectrophotometer at a UV–vis scan rate value of 600 nm/min (HClO λ = 235 and 289 nm; ClO^- λ = 294 nm). Calibration curves were obtained using the sodium hypochlorite pentahydrate ($NaClO{\cdot}5\ H_2O$) supplied by TCI. The concentration of chlorate (ClO_3^-) and perchlorate (ClO_4^-) was evaluated by ion chromatography (IC) analysis. Metrohm 882 compact IC was equipped with a Metrosep A Supp 5–250/4.0. A solution of 1 mM $NaHCO_3$ and 3.2 mM Na_2CO_3 was used as standard eluent and flowed at 0.7 mL/min. Calibration curves were obtained by using the pure standards ClO_3^- (standard ICCLO31, 1000 ppm) and ClO_4^- (standard ICCLO41, 1000 ppm) ISO certificated supplied by Inorganic Ventures.

3. Results and discussion

The electrochemical and electrocatalytic behavior of NiFe-based electrodes was studied in KOH+NaCl to evaluate the possible use of the NiFe NWs electrodes in seawater, and the results were compared with those obtained in KOH.

First of all, CVs at different scan rates were performed to calculate the specific capacitance by the double-layer capacitance method [72]. CVs were carried out with a scan rate from 20 to 40 mV s^{-1}in the potential range from −0.82 V to 1.02 V vs RHE, where no reactions occurred. This test was also carried out on a Ni planar sheet, for comparison.

For each scan rate, the anodic and cathodic current density at 0.975 V vs. RHE, were measured, and the difference was calculated and plotted vs. the scan rate.

The slope of the linear fit represents the specific capacitance that is related to the real active surface area of the electrode. Fig. 1 shows that the slope for NiFe is greater than the slope of Ni sheet, both for KOH and KOH+NaCl. Comparable values were obtained in both solutions. Thus, from planar electrodes to nanostructured ones, the real electrode surface area increases (about 7.8 times). This value is plausible because it is comparable (the total surface area of NWs is 6.26 cm^2, 10.4 times higher than the geometrical one) with the value calculated using the method proposed in [73] based on the analysis of SEM images. Considering the result obtained with the double-layer capacitance method, a specific load on the total surface area of about 0.424 mg/cm^2 can be qualitatively estimated. From the result of Fig. 1, it can be concluded that the NiFe NWs are able to provide higher electrochemical active surface area and, thus more active sites than planar electrodes, improving electrode catalytic activity [74].

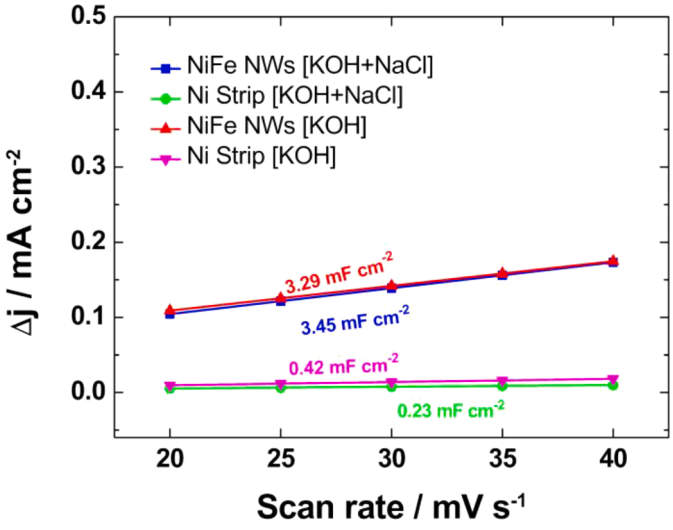

Fig. 1. Specific capacitance of the electrodes evaluated by double layer capacitance method: pink) Ni Strip in KOH and green) in KOH+NaCl; red) NiFe NWs in KOH and blue) in KOH+NaCl.

QSSP tests were carried out for both HER (Fig. 2a) and OER (Fig. 2b). A range of 0.7 V has been analyzed with a scan rate of 0.1667 mV s^{-1}. For both reactions, the QSSP curves recorded in the KOH+NaCl solution exhibit almost no noticeable change when compared with the KOH. The slight differences are due to the increase in the conductivity of the solution due to the addition of NaCl. The values of η_{10} and η_{100} for HER and OER were also measured and reported in Fig. 2c and d. These values are important because they are usually used to compare the electrocatalytic activity of various catalysts [44]. In particular, to achieve a current density of 10 mA cm^{-2} (the most common parameter used for the comparison), the η values in the KOH+NaCl solution are −211 mV for HER and 289 mV OER, respectively. These values are slightly lower than those measured in the KOH alone. Furthermore, with respect to literature data (see Table S2), the values obtained are in line with many NiFe-based electrodes and higher than those obtained with a planar Ni strip. This demonstrates that the electrodes obtained herein have good catalytic properties.

The linear range of QSSP curves, Fig. 3, was fitted with Tafel's equation,

$$\eta = a + b\log i$$

where a and b values are linked to exchange current density and Tafel's curve slope, respectively. The procedure is detailed in the previous works [46]. The Tafel slope value is a significant parameter to evaluate the catalyst activity.

Tafel parameters are listed in Table 1. A good performance was obtained both for HER and OER. The values are comparable to those of NiFe-based catalysts proposed in the literature [75–77] (see Table S2). Moreover, as we have demonstrated in [46], the values obtained with the nanostructured NiFe alloy are higher both with respect to pure NWs of Ni and Fe and, obviously, with respect to a planar sheet of Ni. In the case of the Ni sheet, the better results obtained using NWs are due to the increase in the active surface area of the electrode, which ensures the presence of a high number of active sites available for the electrochemical reactions [35–37]. In addition, the nanostructured alloy performs better than the nanostructures of pure components. In particular, for the OER, the results are promising, as when the Tafel slope of the OER is low, the activity of the electrocatalyst is high [78]. As reported by Louie et al. [50], the presence of Fe in the alloy alters the redox properties of Ni, which is the catalyst for OER. These authors have shown that as the Fe content in the alloy increases, there is a shift (to higher anodic values) in the redox potential of the $Ni(OH)_2$ /NiOOH reaction. This leads to a decrease in the average oxidation state of the Ni sites and hence an increase in the activity of the Ni cations for OER.

It is important to note that, in the KOH+NaCl solution test, the Tafel parameter values remain close to those obtained in pure KOH. indicating that the presence of NaCl does not affect the electrocatalytic behavior of the NiFe nanostructured electrodes. The slope values for HER are close to 120 mV suggesting that the rate-determining step is the Volmer step [35]. In the case of OER, a Tafel slope of approximately 40 mV suggests that the adsorption of hydroxide ions on the active site of the catalyst is responsible for determining the rate [78].

The value of turnover frequency (TOF), Table 2, was calculated using the following equation

$$TOF = \frac{iA}{xnF}$$

where i is the current density, in A cm^{-2}, measured at a specific overpotential, A is the geometrical surface area of the electrode, F is the Faraday constant equal to 96,485 C mol^{-1}, x is the number of transferred electrons for each molecule of gas produced (x = 2 for HER, x = 4 for

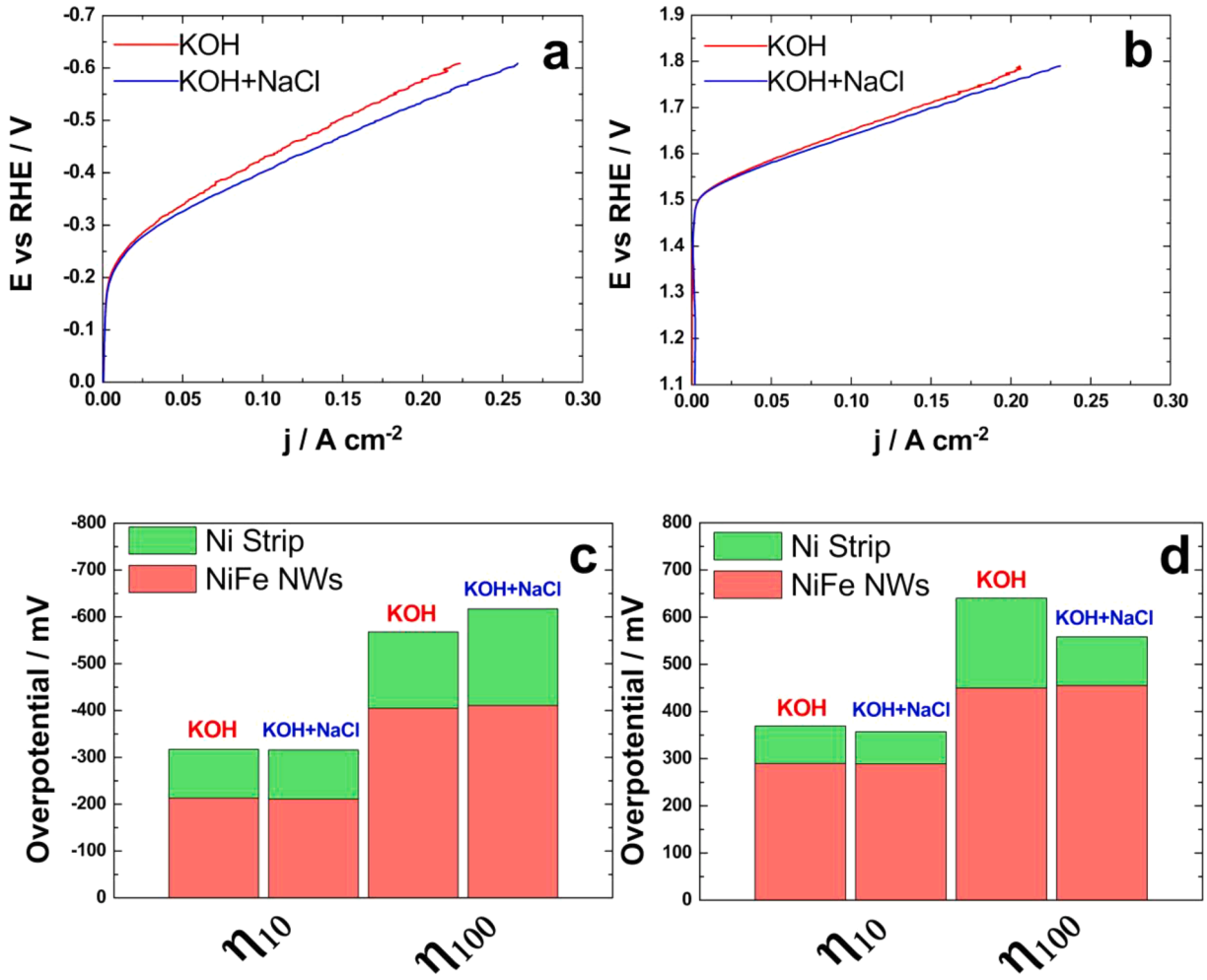

Fig. 2. QSSP for (a) HER and (b) OER at 0.1667 mV s^{-1} in KOH+NaCl (blue) and in KOH (red) aqueous solution. Values of η_{10} and η_{100} for HER (c) and OER (d).

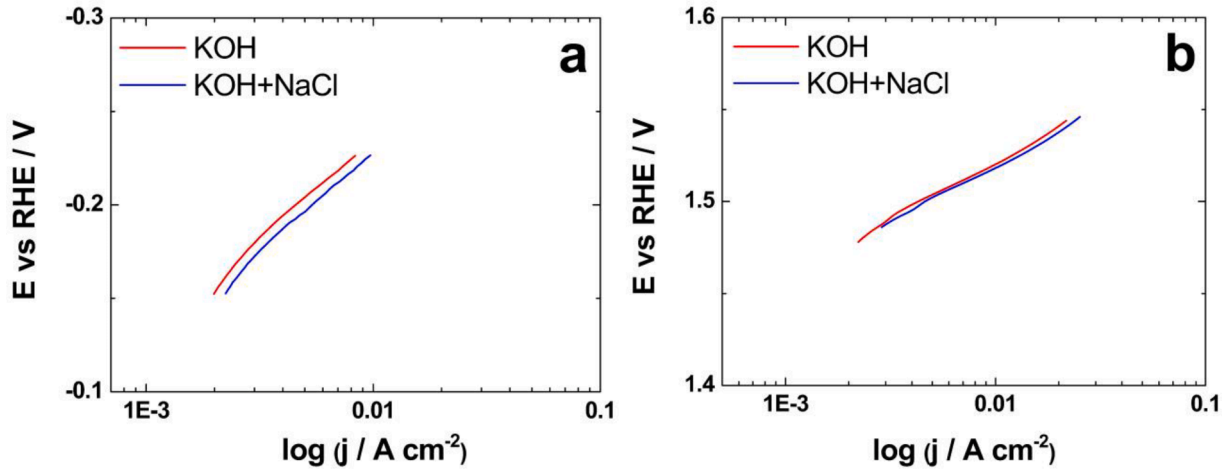

Fig. 3. Linearity range of QSSP curves for both (a) HER and (b) OER in KOH+NaCl (blue) and in KOH (red) aqueous solution.

OER), *n* is the number of moles of NiFe, assuming that all metal sites are involved in gas evolution reaction [79]. The value of TOF related to HER and OER on a Ni planar sheet was also reported for comparison. The TOF value is an interesting parameter because it is used to evaluate the effect of catalyst morphology on its activity [79,80]. In fact, the TOF is directly correlated to the active sites of electrocatalysts. The calculated TOF value for the nanostructured alloy is higher than the Ni planar sheet. As reported by Silva et al. [79], this can be attributable to the high availability of active sites. The TOF values, calculated at η_{400}, are comparable with those reported for NiFe-based electrodes [80].

Galvanostatic step polarization tests were performed to study the behavior at different current densities. Different constant current densities (0.01, 0.02, 0.05, 0.1, 0.2, 0.5 A cm^{-2}) are applied for five minutes. Each point in the graph represents the average value of the measured

Table 1
Fitted Tafel's parameters for HER and OER in KOH and KOH+NaCl solutions.

Solution	HER			OER		
	a (V)	*b* (V)	R^2 (%)	*a* (V)	*b* (V)	R^2 (%)
KOH	−0.46	−0.114	99.2	1.62	0.045	99.6
KOH+NaCl	−0.45	−0.110	99.4	1.63	0.043	99.8

Table 2
TOF values for NiFe NWs and Ni planar strip in KOH and KOH+NaCl solutions.

	TOF [s^{-1}] HER per η=400 mV	TOF [s^{-1}] OER per η=400 mV
Ni strip KOH	6.62×10^{-5}	2.5×10^{-5}
Ni strip KOH+NaCl	2.28×10^{-5}	3.31×10^{-5}
NiFe NWs KOH	0.007	0.00366
NiFe NWs KOH+NaCl	0.0089	0.0041

potential.

As shown in Fig. 4, the catalyst exhibits good catalytic activity both for HER and OER. The performance of the catalyst in the KOH+NaCl solution is very close to that in the KOH electrolyte. This result for the anodic side suggests a selective OER under these experimental conditions. At 10 mA cm^{-2}, for KOH+NaCl, the potential is around −0.21 and 1.53 V vs. RHE for HER and OER, respectively.

To evaluate the mid-term behavior of the electrodes, a constant current density of −50 mA cm^{-2} for HER and 50 mA cm^{-2} for OER, respectively, was applied for 6 h The results are shown in Fig. 5. Each point in the graphs is the value of the potential averaged over 1800 s. It can be seen how the potential is almost constant, and there is no difference between the two investigated solutions. For the HER tests in KOH+NaCl, at the beginning, the potential is −0.32 V vs. RHE, and at the end, it is −0.335 V vs. RHE. There is a loss of 15 mV, which is a promising result. The NiFe nanostructured electrodes also showed good behavior for OER. During the test, there is a loss of about 10 mV, with a final potential of 1.61 V.

To better evaluate the electrode stability, especially in the KOH+NaCl solution, the previous test was repeated for 125 h The potential values are very similar to those obtained with the mid-term test. In fact, as shown in Fig. 6a, the cathodic potential is about −0.33 V vs. RHE, and this value remained almost constant throughout the test for both investigated solutions.

For OER, in the beginning, the two curves are almost overlapped. After about 75 h, the potential in KOH+NaCl is slightly higher than the potential in KOH, with a final value of 1.63 V vs. RHE. Furthermore, insignificant variations occur in the potential throughout the entire test, as demonstrated in Fig. 6b. It is very important to note that this value is lower than the hypochlorite standard reduction potential. In particular, the standard electrode potential of hypochlorite reaction.

$$2\ OH^- + Cl^- \rightarrow ClO^- + H_2O + 2\ e^-$$

is pH dependent, and at pH 14, the value is 1.714 V vs. RHE [81]. From these results, it can be concluded that in our experimental conditions, the potential of Cl^- oxidation was not reached, and thus only the OER in the KOH+NaCl solution occurs [65].

The electrolytic solution after the long-term stability electrolysis was analyzed to confirm the absence of hypochlorite (OCl^-) and other chlorine compounds (HClO, ClO_3^-, ClO_4^-). UV–vis spectroscopy at a scan rate value of 600 nm/min was used to check the presence of ClO^- and HClO. Fig. S2 shows the chromatogram achieved by analyzing a standard ClO^- and HClO solution and the electrolytic solution before and after the long-term stability test. As reported in [82], the wavelengths of absorbance (λ) of ClO^- and HClO are 294 nm and 235/289 nm, respectively, which is in line with our results (Fig. S3). According to these analyses, no ClO^- or HClO was observed, thus confirming their absence in the electrolytic solution after long-term stability electrolysis. In addition, ion chromatography was used to detect ClO_3^- and ClO_4^-. Fig. S3 shows the chromatogram of the standard solution of ClO_3^- and ClO_4^-, and of the electrolytic solutions before and after long-term stability electrolysis. In the case solution used for the long-term stability electrolysis, only one peak was observed at a retention time of approximately 9 min, which is related to the chloride ions, while no other peaks were observed, thus confirming the absence of ClO_3^- and ClO_4^-. Thus, NiFe NWs electrodes can operate as bifunctional catalysts in seawater electrolyzers thanks to their selectivity to OER. Other works obtained similar results using different NiFe-based catalysts [58,76,83].

Furthermore, although the long-term stability tests were performed for 125 h, electrodes are mechanically and chemically stable. This result was confirmed by different analyses performed before and after the long-term stability tests. Fig. 7 shows the SEM image of the electrode before the test.

The morphology is typical of the NWs, which have an almost regular cylindrical shape, obtained using a polycarbonate membrane as a template. Fig. 7a shows the top view of the nanostructured electrode, Fig. 7b and c shows the cross-sectional view, while in Fig. 7d, the tilted top view is reported. In Fig. 7a, it can be observed that the Ni current collector is uniformly covered by NiFe NWs. The Ni collector, about 12 μm thick, is continuous, uniform, and free of cracks or fractures. The

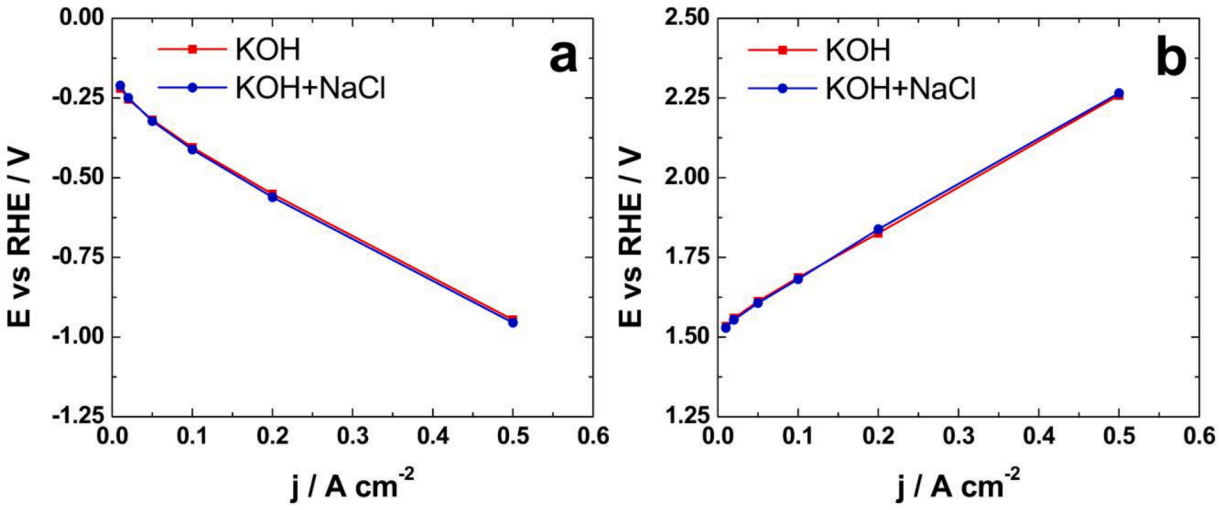

Fig. 4. Galvanostatic-step polarization for (a) HER and (b) OER in KOH+NaCl (blue) and in KOH (red) aqueous solution.

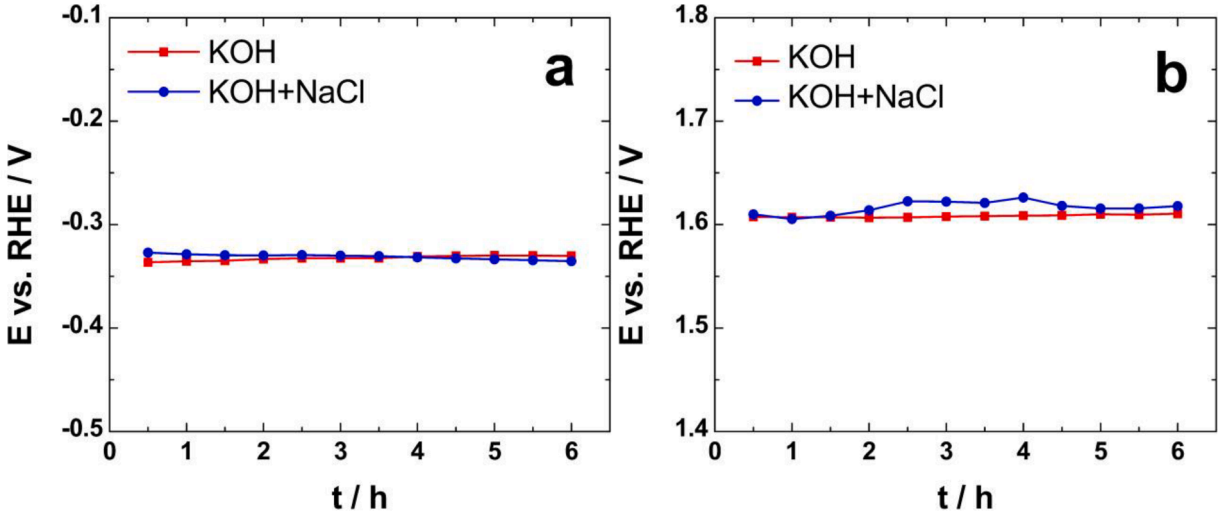

Fig. 5. Mid-term stability test for 6 h for (a) HER at −50 mA cm^{-2} and b) OER at 50 mA cm^{-2} in KOH+NaCl (blue) and in KOH (red) aqueous solution.

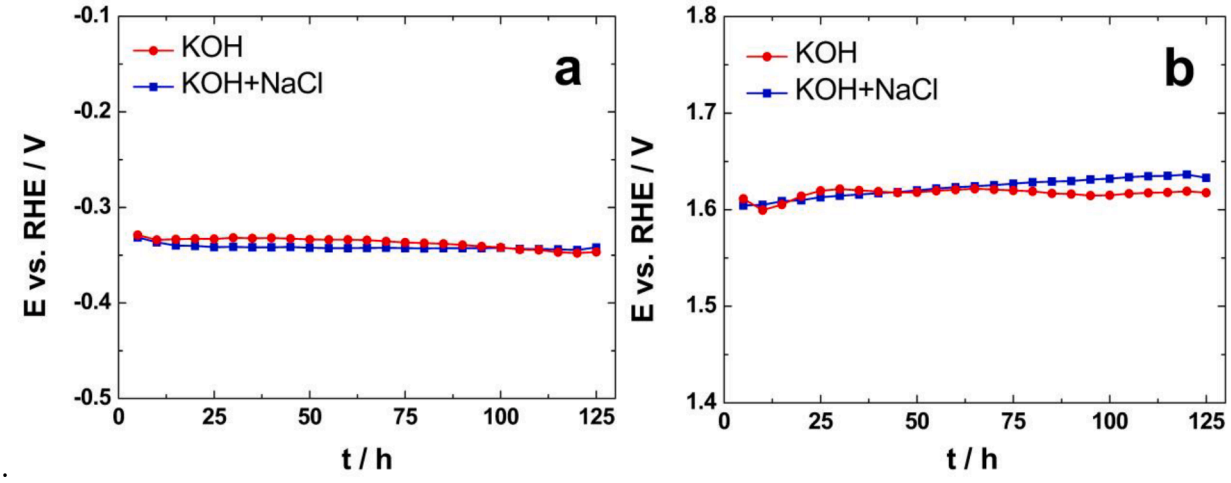

Fig. 6. Long-term stability test for 125 h for (a) HER at −50 mA cm^{-2} and (b) OER at 50 mA cm^{-2} in KOH+NaCl (blue) and in KOH (red) aqueous solution.

interconnections between different wires, Fig. 7a and d, are due to the shape of the nanochannels of the polycarbonate template. Fig. 7b and c shows that NWs are firmly connected to the current collector. These NWs have a low surface roughness, a diameter of 220–250 nm, and a length of 12 μm. The presence of some broken NWs, Fig. 7c, is due to the preparation of the cross-section of the sample for SEM analysis, which was obtained by simply tearing off a flap of the sample. The EDS before the long-term stability test shows only the presence of Fe and Ni peaks (Fig. S4). The Fe content is about 79%. The iron content is about 2.85 times that of nickel, in agreement with the well-known anomalous co-deposition of the two elements [46,84].

After the long-term stability test in the KOH+NaCl solution, no particular differences were observed either in the morphology and in the composition of the NWs both in the electrodes used for HER (Fig. 8a and c) and for those used for OER (Fig. 8b and d). In fact, SEM images (Fig. 8a and b) showed that nanostructure morphology remained almost unchanged without collapse, demonstrating that these nanostructure arrays are stable. Besides, only Ni and Fe peaks are detected in the EDS spectra (Fig. 8c and d). The K peak in the spectrum of Fig. 8d is due to traces of KOH formed by precipitation on the electrode when it is disassembled from the electrolysis cell and dried in air. These results suggest long-time durability of the NiFe NWs-based electrodes.

Nanostructured electrodes were also characterized by XRD, as shown in Fig. 9. In the as-prepared electrode, the peaks at about 43.23°, 50.38°, 74.18° and 90.16° can be ascribed to the reflections from (111), (200), (220), and (311) planes of the face-centered cubic structure of the Fe-Ni alloy (card no. 47-1405) [84–86]. The 200 reflections have a high intensity. This means NiFe NWs are grown with a preferred orientation in the ⟨100⟩ direction. This behavior was also observed and proved by theoretical calculations for Au e Cu NWs obtained by template pulsed electrodeposition into polycarbonate membranes [87]. As reported in the experimental section NiFe NWs were obtained by switching the potential between −1.35 V and −0.65 V vs. SCE (Fig. S1). For these potential values, an inversion of the polarity of the deposition current density occurs, which is responsible for the preferential growth of the nanostructures. In particular, the preferential ⟨100⟩ growth direction is due to the preferential dissolution, during the pulse with anodic current density, of the surface grown in the other directions. Ni peaks, coming from the Ni current collector, were also observed at 44.53°, 51,86° and 76.37° They are correlated to α-Ni face-centered cubic structure (card no. 04-850) and can be referred to the reflections from (111), (200) and (220) planes. XRD spectra remain practically unchanged after long-term stability testing confirming SEM and EDS results and thus the stability of the nanostructured NiFe electrodes.

The surface of electrodes was chemically characterized by means of X-ray Photoelectron Spectroscopy (XPS) before and after the long-term

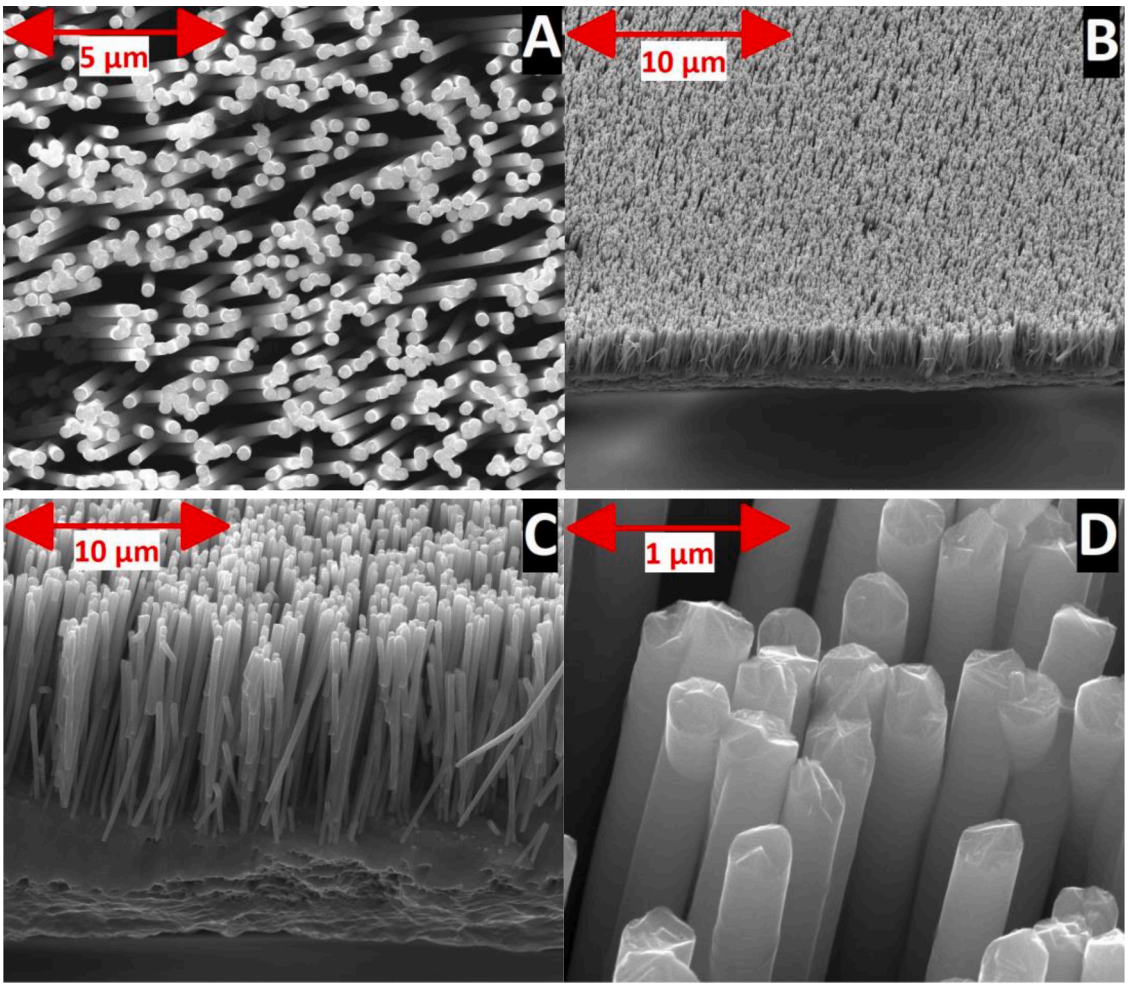

Fig. 7. a-d) SEM images of NiFe NWs electrode before long-term stability test. (a) top view; b-c) tilted cross-sectional view and d) tilted top view.

stability test OER in KOH+NaCl, Fig. 10 (Table S1). A direct comparison between the quantitative superficial analysis is not possible, partially due to the different air exposure of the samples, altering the (adventitious) carbon content, and partially due to the non-homogeneous nature of the samples. NWs may alter the inelastic mean free path of the electrons throughout the analyzed samples and allow the collection of electrons from lower layers. Nevertheless, after the long-term stability test in KOH+NaCl, it was possible to observe the presence of both K and Cl on the electrode surface of the sample. The observed Cl is only in the chloride form. The C 1s region analysis also showed the presence of carbonate species precipitated on the electrode surface after the long-term stability test. On the metal side, it has been possible to observe that both Fe and Ni are present in a distribution of chemical environments. The as-prepared electrode shows a distribution of metallic Fe (ca. 23%) and Fe(II) (FeO, $NiFeO_2$), and Fe(III) (FeOOH) species. The presence of high spin Fe(III) compounds is also confirmed by the presence of the satellite feature around 720 eV Such species distribution is somehow maintained after the long-term stability test in KOH+NaCl, but the overall Fe distribution varies, lowering the Fe(0) content to about 9% and lowering the intensity of the satellite feature (suggesting a decrease in Fe(III) content). Observing the Ni $2p_{3/2}$ spectra (Fig. 10, right), it is possible to observe that, after the long-term stability test, the electrode nanowires surface appears to be constituted mainly of oxidized Ni, in the form of $Ni(OH)_2$.

In order to avoid the introduction of calculus artifacts, the spectral analysis was carried out tracking mainly the species' main peaks and leaving the expected multiplet pattern of Ni as a combination of contributions from all observed species. As such, the observed alteration of the multiplet pattern before and after the long-term stability test is attributable to a non-homogeneous distribution of Ni-oxidized sites. Our findings are confirmed by the O 1s region analysis (also showing the presence of physisorbed H_2O and chemisorbed O_2; see supporting info).

Finally, to summarize our results and to better compare with others, in Table S2, the more relevant and recent literature data were listed. The data analysis shows that the performances of NiFe NWs described are very close to those obtained by other authors in the case of NiFe-based electrodes. It is important to highlight that our tests were conducted at room temperature. Consequently, the performances that we have obtained can be improved if we increase the operating temperature. In Table S2, the value of the mass activity, calculated as the ratio between the current density (A cm^{-2}) and the catalyst loading (mg cm^{-2}), was reported. For our electrode, at 10 mA cm^{-2}, the mass activity is 3.02×10^{-3} A mg^{-1}. The value of the mass activity is important because it allow us to compare the activity of different catalysts per unit of mass. As shown in Table S2, the obtained value for HER is comparable to Ni-based compounds.

4. Conclusions

Nanostructured electrodes of NiFe alloy obtained by template electrosynthesis were studied in 30% w/w KOH + 0.5 M NaCl solution to investigate their suitability for seawater electrolysis. A nanostructured alloy with about 79% Fe was investigated as a cathode and anode for water electrolysis at room temperature. The behavior of electrodes in KOH alone was also studied for comparison. The electrochemical behavior was studied by CV, QSSP and galvanostatic tests. The stability

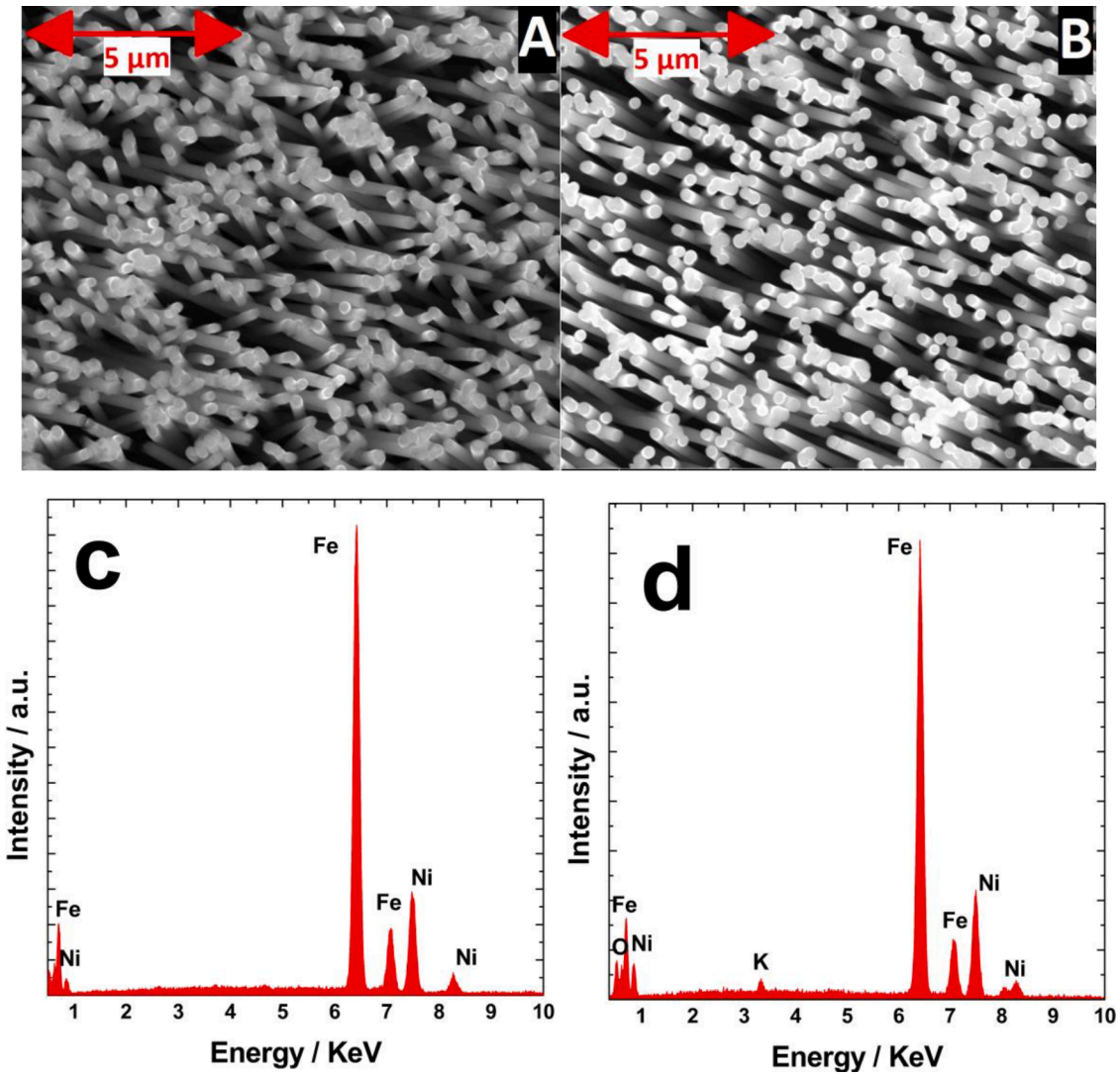

Fig. 8. SEM images and EDS of NiFe NWs electrodes after long-term stability test in KOH+NaCl: a, c) HER and b, d) OER.

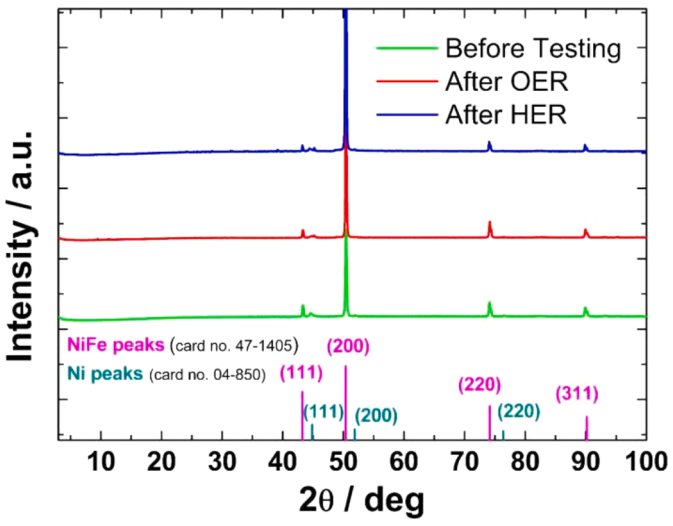

Fig. 9. XRD patterns of NiFe NWs electrodes: green) before testing; red) after long-term stability test HER in KOH+NaCl; and blue) after a long-term stability test OER in KOH+NaCl.

of the nanostructured electrodes was evaluated by mid- and long-term galvanostatic tests performed at a current density of ±50 mA cm^{-2} for 6 and 125 h, respectively. Furthermore, a chemical–physical characterization was carried out after the long-term galvanostatic tests to detect any potential alterations in the morphology and composition of the electrodes. In addition, the KOH + 0.5 M NaCl solutions were analyzed after the long-term galvanostatic tests to investigate the possible formation presence of chlorine compounds on the anode side.

All obtained results showed that the NiFe nanostructured electrodes exhibit good catalytic activity both for HER and OER, and the presence of NaCl doesn't affect their electrocatalytic behavior. In fact, the performance of the catalyst in the KOH+NaCl solution is very close to that in the KOH electrolyte. Additionally, the electrodes demonstrated mechanical and chemical stability during both medium and long-term gas development. During the galvanostatic tests at +50 mA cm^{-2}, the potential value measured for the oxygen evolution reaction was always lower than the thermodynamic redox potential for the hypochlorite formation reaction. The solution used for the long-term galvanostatic test was analyzed to confirm the absence of chlorine compounds. These findings indicate that under the experimental conditions, there is a selective oxygen evolution reaction on the anodic side. Therefore, these electrodes hold potential for electrolysis in seawater.

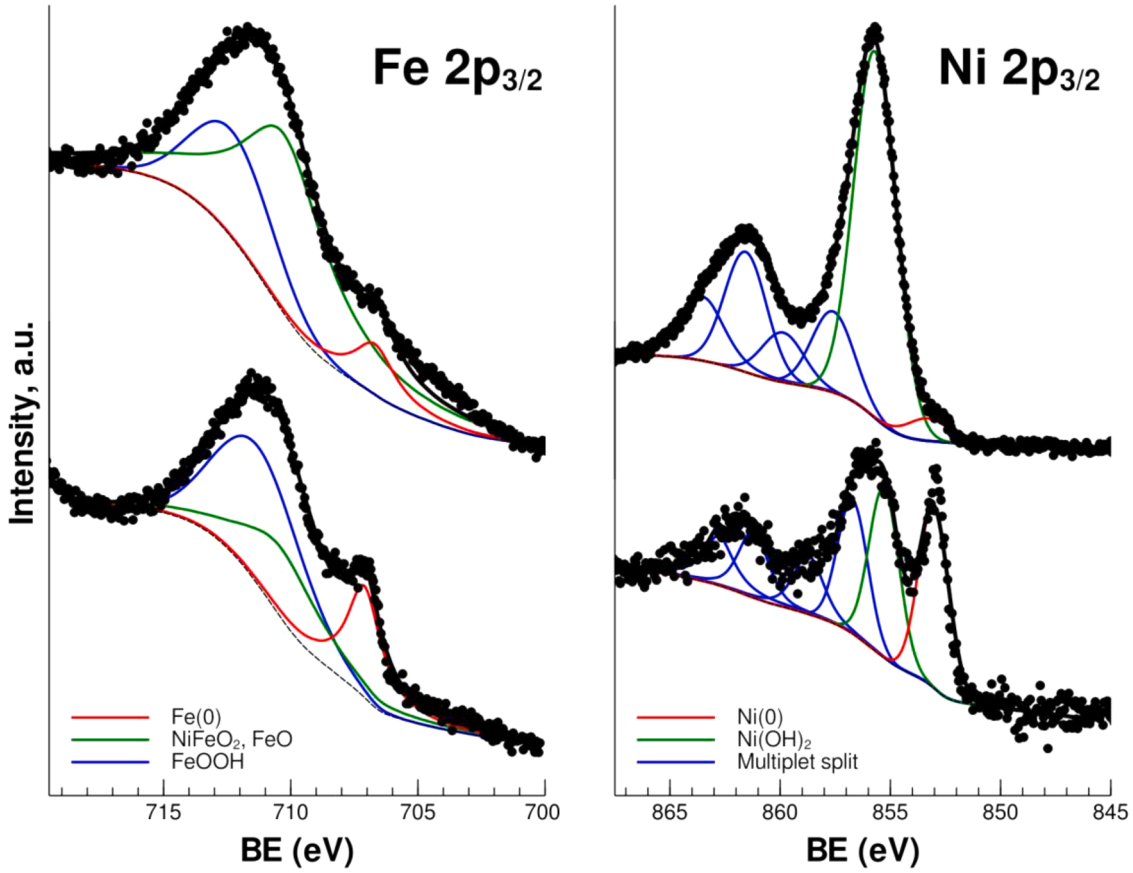

Fig. 10. XPS spectra in the Fe $2p_{3/2}$ (left) and Ni $2p_{3/2}$ (right) regions, before (bottom) and after the long-term stability test (top).

CRediT authorship contribution statement

S. Carbone: Methodology, Investigation, Validation, Writing – original draft. **F. Proietto:** Methodology, Investigation, Validation, Writing – original draft. **F. Bonafede:** Methodology, Investigation, Validation. **R.L. Oliveri:** Validation, Writing – review & editing. **B. Patella:** Methodology, Investigation, Validation. **F. Ganci:** Validation, Writing – review & editing. **G. Aiello:** Validation, Writing – review & editing. **P. Mandin:** Conceptualization, Writing – review & editing, Supervision. **M. Kim:** Conceptualization, Writing – review & editing, Supervision. **M. Scopelliti:** Investigation, Writing – review & editing. **R. Inguanta:** Project administration, Funding acquisition, Writing – review & editing, Supervision.

Declaration of Competing Interest

The authors declare that they have no known competing financial interests or personal relationships that could have appeared to influence the work reported in this paper.

Data availability

Data will be made available on request.

Acknowledgments

This work was partially financed by the project "SiciliAn Micro-nanOTecH Research And Innovation CEnter "SAMOTHRACE" (MUR, PNRR-M4C2, ECS_00000022), spoke 3 - Università degli Studi di Palermo "S2-COMMs - Micro and Nanotechnologies for Smart & Sustainable Communities". The Advanced Technologies Network (ATeN) Center (University of Palermo) is also acknowledged for XPS measurements.

Supplementary materials

Supplementary material associated with this article can be found, in the online version, at doi:10.1016/j.electacta.2023.143120.

References

[1] D. Gielen, F. Boshell, D. Saygin, M.D. Bazilian, N. Wagner, R. Gorini, The role of renewable energy in the global energy transformation, Energy Strategy Rev. 24 (2019) 38–50, https://doi.org/10.1016/j.esr.2019.01.006.
[2] P.A. Owusu, S. Asumadu-Sarkodie, A review of renewable energy sources, sustainability issues and climate change mitigation, Cogent Eng. 3 (2016), 1167990, https://doi.org/10.1080/23311916.2016.1167990.
[3] A. Baldinelli, L. Barelli, G. Bidini, G. Cinti, A. Di Michele, F. Mondi, How to power the energy-water nexus: coupling desalination and hydrogen energy storage in mini-grids with reversible solid oxide cells, Processes 8 (2020) 1494, https://doi.org/10.3390/pr8111494.
[4] D. Falabretti, M. Lindholm, M. Merlo, G. Scapeccia, Energy storage coupling in a high efficiency household scenario: a real life experimental application, J. Energy Storage 17 (2018) 496–506, https://doi.org/10.1016/j.est.2018.04.010.
[5] P. Marocco, D. Ferrero, A. Lanzini, M. Santarelli, Optimal design of stand-alone solutions based on RES + hydrogen storage feeding off-grid communities, Energy Convers. Manag. 238 (2021), 114147, https://doi.org/10.1016/j.enconman.2021.114147.
[6] P. Hou, P. Enevoldsen, J. Eichman, W. Hu, M.Z. Jacobson, Z. Chen, Optimizing investments in coupled offshore wind -electrolytic hydrogen storage systems in Denmark, J. Power Sources 359 (2017) 186–197, https://doi.org/10.1016/j.jpowsour.2017.05.048.
[7] K. Oshiro, S. Fujimori, Role of hydrogen-based energy carriers as an alternative option to reduce residual emissions associated with mid-century decarbonization goals, Appl. Energy 313 (2022), 118803, https://doi.org/10.1016/j.apenergy.2022.118803.
[8] H. Nami, O.B. Rizvandi, C. Chatzichristodoulou, P.V. Hendriksen, H.L. Frandsen, Techno-economic analysis of current and emerging electrolysis technologies for

green hydrogen production, Energy Convers. Manag. 269 (2022), 116162, https://doi.org/10.1016/j.enconman.2022.116162.
[9] https://www.irena.org/Energy-Transition/Technology/Hydrogen n.d.
[10] Y. Peng, Y. Liao, D. Ye, Z. Meng, R. Wang, S. Zhao, et al., Recent advances regarding precious metal-based electrocatalysts for acidic water splitting, Nanomaterials 12 (2022) 2618, https://doi.org/10.3390/nano12152618.
[11] D.M.F. Santos, C.A.C. Sequeira, J.L. Figueiredo, Hydrogen production by alkaline water electrolysis, Quím Nova 36 (2013) 1176–1193, https://doi.org/10.1590/S0100-40422013000800017.
[12] P.M. Bodhankar, P.B. Sarawade, G. Singh, A. Vinu, D.S. Dhawale, Recent advances in highly active nanostructured NiFe LDH catalyst for electrochemical water splitting, J. Mater. Chem. A 9 (2021) 3180–3208, https://doi.org/10.1039/D0TA10712C.
[13] G. Maduraiveeran, M. Sasidharan, W Jin, Earth-abundant transition metal and metal oxide nanomaterials: synthesis and electrochemical applications, Prog Mater. Sci. 106 (2019), 100574, https://doi.org/10.1016/j.pmatsci.2019.100574.
[14] K. Su, Z. Yu, M. Li, S. Yang, Y. Liang, Y. Tang, et al., Three-dimensional nickel cobalt phosphide nanocrosses with well-defined axial arms for efficient oxygen evolution reaction, Chem. A Eur. J. (2023), e202300398, https://doi.org/10.1002/chem.202300398.
[15] L. Bruno, M. Scuderi, F. Priolo, L. Falciola, S. Mirabella, Enlightening the bimetallic effect of Au@Pd nanoparticles on Ni oxide nanostructures with enhanced catalytic activity, Sci. Rep. 13 (2023) 3203, https://doi.org/10.1038/s41598-023-29679-6.
[16] L. Silipigni, F. Barreca, E. Fazio, F. Neri, T. Spanò, S. Piazza, et al., Template electrochemical growth and properties of Mo oxide nanostructures, J. Phys. Chem. C 118 (2014) 22299–22308, https://doi.org/10.1021/jp505819j.
[17] P.G. Bruce, B. Scrosati, J.-M. Tarascon, Nanomaterials for rechargeable lithium batteries, Angew. Chem. Int. Ed. 47 (2008) 2930–2946, https://doi.org/10.1002/anie.200702505.
[18] R. Inguanta, E. Rinaldo, S. Piazza, C Sunseri, Lead nanowires for microaccumulators obtained through indirect electrochemical template deposition, Electrochem. Solid-State Lett. 13 (2010) K1, https://doi.org/10.1149/1.3246944.
[19] M.G. Insinga, R.L. Oliveri, C. Sunseri, R. Inguanta, Template electrodeposition and characterization of nanostructured Pb as a negative electrode for lead-acid battery, J. Power Sources 413 (2019) 107–116, https://doi.org/10.1016/j.jpowsour.2018.12.033.
[20] G. Mineo, M. Scuderi, G. Pezzotti Escobar, S. Mirabella, E Bruno, Engineering of nanostructured WO_3 powders for asymmetric supercapacitors, Nanomaterials 12 (2022) 4168, https://doi.org/10.3390/nano12234168.
[21] M. Urso, F. Priolo, S. Mirabella, Investigating the charge-discharge behaviour of Ni $(OH)_2$ nanowalls, Appl. Surf. Sci. 534 (2020), 147585, https://doi.org/10.1016/j.apsusc.2020.147585.
[22] P.G. Perret, P.R.L. Malenfant, C. Bock, B. MacDougall, Electro-deposition and dissolution of MnO_2 on a graphene composite electrode for its utilization in an aqueous based hybrid supercapacitor, J. Electrochem. Soc. 159 (2012) A1554–A1561, https://doi.org/10.1149/2.064208jes.
[23] P. Perret, Z. Khani, T. Brousse, D. Bélanger, D. Guay, Carbon/PbO_2 asymmetric electrochemical capacitor based on methanesulfonic acid electrolyte, Electrochim. Acta 56 (2011) 8122–8128, https://doi.org/10.1016/j.electacta.2011.05.125.
[24] X. Qu, P.J.J. Alvarez, Q. Li, Applications of nanotechnology in water and wastewater treatment, Water Res. 47 (2013) 3931–3946, https://doi.org/10.1016/j.watres.2012.09.058.
[25] C. Zhu, G. Yang, H. Li, D. Du, Y. Lin, Electrochemical sensors and biosensors based on nanomaterials and nanostructures, Anal. Chem. 87 (2015) 230–249, https://doi.org/10.1021/ac5039863.
[26] W. Xia, A. Mahmood, Z. Liang, R. Zou, S. Guo, Earth-abundant nanomaterials for oxygen reduction, Angew. Chem. Int. Ed. 55 (2016) 2650–2676, https://doi.org/10.1002/anie.201504830.
[27] C. Zhu, H. Li, S. Fu, D. Du, Y. Lin, Highly efficient nonprecious metal catalysts towards oxygen reduction reaction based on three-dimensional porous carbon nanostructures, Chem. Soc. Rev. 45 (2016) 517–531, https://doi.org/10.1039/C5CS00670H.
[28] R. Inguanta, S. Piazza, C. Sunseri, A. Cino, V. Di Dio, D.L. Cascia, et al., An electrochemical route towards the fabrication of nanostructured semiconductor solar cells. SPEEDAM 2010, IEEE, Pisa, Italy, 2010, pp. 1166–1171, https://doi.org/10.1109/SPEEDAM.2010.5542264.
[29] E. Roduner, Size matters: why nanomaterials are different, Chem. Soc. Rev. 35 (2006) 583, https://doi.org/10.1039/b502142c.
[30] A.B. Asha, R. Narain, Nanomaterials properties. Polymer Science and Nanotechnology, Elsevier, 2020, pp. 343–359, https://doi.org/10.1016/B978-0-12-816806-6.00015-7.
[31] B. Ni, X. Wang, Face the edges: catalytic active sites of nanomaterials, Adv. Sci. 2 (2015), 1500085, https://doi.org/10.1002/advs.201500085.
[32] H. Zhang, Z. Feng, L. Wang, D. Li, P. Xing, Bifunctional nanoporous Ni-Zn electrocatalysts with super-aerophobic surface for high-performance hydrazine-assisted hydrogen production, Nanotechnology 31 (2020), 365701, https://doi.org/10.1088/1361-6528/ab9396.
[33] L. Bruno, S. Battiato, M. Scuderi, F. Priolo, A. Terrasi, S. Mirabella, Physical insights into alkaline overall water splitting with NiO microflowers electrodes with ultra-low amount of Pt catalyst, Int. J. Hydrogen Energy 47 (2022) 33988–33998, https://doi.org/10.1016/j.ijhydene.2022.08.005.
[34] L. Bruno, M. Scuderi, F. Priolo, S. Mirabella, Enhanced electrocatalytic activity of low-cost NiO microflowers on graphene paper for the oxygen evolution reaction, Sustain. Energy Fuels 6 (2022) 4498–4505, https://doi.org/10.1039/D2SE00829G.
[35] G.B. Darband, Recent advances in methods and technologies for enhancing bubble detachment during electrochemical water splitting, Renew. Sustain. Energy Rev. (2019) 21.
[36] R. Wen, S. Xu, X. Ma, Y.-C. Lee, R Yang, Three-dimensional superhydrophobic nanowire networks for enhancing condensation heat transfer, Joule 2 (2018) 269–279, https://doi.org/10.1016/j.joule.2017.11.010.
[37] S.H. Ahn, I. Choi, H.-Y. Park, S.J. Hwang, S.J. Yoo, E. Cho, et al., Effect of morphology of electrodeposited Ni catalysts on the behavior of bubbles generated during the oxygen evolution reaction in alkaline water electrolysis, Chem. Commun. 49 (2013) 9323, https://doi.org/10.1039/c3cc44891f.
[38] R.A. McIntyre, Common nano-materials and their use in real world applications, Sci. Prog. 95 (2012) 1–22, https://doi.org/10.3184/003685012X13294715456431.
[39] N. Tian, J. Xiao, Z.-Y. Zhou, H.-X. Liu, Y.-J. Deng, L. Huang, et al., Pt-group bimetallic nanocrystals with high-index facets as high performance electrocatalysts, Faraday Discuss. 162 (2013) 77, https://doi.org/10.1039/c3fd20146e.
[40] H. Wang, Y. Yang, F.J. DiSalvo, H.D Abruña, Multifunctional electrocatalysts: ru–M (M = Co, Ni, Fe) for alkaline fuel cells and electrolyzers, ACS Catal. 10 (2020) 4608–4616, https://doi.org/10.1021/acscatal.9b05621.
[41] W. Sheng, A.P. Bivens, M. Myint, Z. Zhuang, R.V. Forest, Q. Fang, et al., Non-precious metal electrocatalysts with high activity for hydrogen oxidation reaction in alkaline electrolytes, Energy Environ. Sci. 7 (2014) 1719–1724, https://doi.org/10.1039/C3EE43899F.
[42] J. Mohammed-Ibrahim, X. Sun, Recent progress on earth abundant electrocatalysts for hydrogen evolution reaction (HER) in alkaline medium to achieve efficient water splitting - a review, J. Energy Chem. 34 (2019) 111–160, https://doi.org/10.1016/j.jechem.2018.09.016.
[43] F. Ganci, B. Patella, E. Cannata, V. Cusumano, G. Aiello, C. Sunseri, et al., Ni alloy nanowires as high efficiency electrode materials for alkaline electrolysers, Int. J. Hydrogen Energy 46 (2021) 35777–35789, https://doi.org/10.1016/j.ijhydene.2020.11.208.
[44] J. Zhu, L. Hu, P. Zhao, L.Y.S. Lee, K.-Y. Wong, Recent advances in electrocatalytic hydrogen evolution using nanoparticles, Chem. Rev. 120 (2020) 851–918, https://doi.org/10.1021/acs.chemrev.9b00248.
[45] M.-I. Jamesh, X. Sun, Recent progress on earth abundant electrocatalysts for oxygen evolution reaction (OER) in alkaline medium to achieve efficient water splitting - a review, J. Power Sources 400 (2018) 31–68, https://doi.org/10.1016/j.jpowsour.2018.07.125.
[46] B. Buccheri, F. Ganci, B. Patella, G. Aiello, P. Mandin, R. Inguanta, Ni-Fe alloy nanostructured electrodes for water splitting in alkaline electrolyser, Electrochim. Acta 388 (2021), 138588, https://doi.org/10.1016/j.electacta.2021.138588.
[47] I. Flis-Kabulska, J. Flis, Electroactivity of Ni-Fe cathodes in alkaline water electrolysis and effect of corrosion, Corros. Sci. 112 (2016) 255–263, https://doi.org/10.1016/j.corsci.2016.07.017.
[48] K. Fominykh, P. Chernev, I. Zaharieva, J. Sicklinger, G. Stefanic, M. Döblinger, et al., Iron-doped nickel oxide nanocrystals as highly efficient electrocatalysts for alkaline water splitting, ACS Nano 9 (2015) 5180–5188, https://doi.org/10.1021/acsnano.5b00520.
[49] M. Gong, Y. Li, H. Wang, Y. Liang, J.Z. Wu, J. Zhou, et al., An advanced Ni-Fe layered double hydroxide electrocatalyst for water oxidation, J. Am. Chem. Soc. 135 (2013) 8452–8455, https://doi.org/10.1021/ja4027715.
[50] M.W. Louie, A.T. Bell, An investigation of thin-film Ni-Fe oxide catalysts for the electrochemical evolution of oxygen, J. Am. Chem. Soc. 135 (2013) 12329–12337, https://doi.org/10.1021/ja405351s.
[51] E. Gonzalez, L. Avaca, A. Carubelli, A. Tanaka, G. Tremiliosifilho, The hydrogen evolution reaction on mild steel and nickel-iron codeposits in alkaline media, Int. J. Hydrogen Energy 9 (1984) 689–693, https://doi.org/10.1016/0360-3199(84)90266-0.
[52] J. De Carvalho, G. Tremiliosi Filho, L.A. Avaca, E.R Gonzalez, Electrodeposits of iron and nickel-iron for hydrogen evolution in alkaline solutions, Int. J. Hydrogen Energy 14 (1989) 161–165, https://doi.org/10.1016/0360-3199(89)90049-9.
[53] S. Zhu, G. Duan, C. Chang, Y. Chen, Y. Sun, Y. Tang, et al., Fast electrodeposited nickle-iron hydroxide nanosheets on sintered stainless steel felt as bifunctional electrocatalyts for overall water splitting, ACS Sustain. Chem. Eng. 8 (2020) 9885–9895, https://doi.org/10.1021/acssuschemeng.0c03017.
[54] B. Zhang, C. Zhu, Z. Wu, E. Stavitski, Y.H. Lui, T.-H. Kim, et al., Integrating Rh species with NiFe-layered double hydroxide for overall water splitting, Nano Lett. 20 (2020) 136–144, https://doi.org/10.1021/acs.nanolett.9b03460.
[55] C. Cheng, F. Liu, D. Zhong, G. Hao, G. Liu, J. Li, et al., Three-dimensional self-supporting catalyst with NiFe alloy/oxyhydroxide supported on high-surface cobalt hydroxide nanosheet array for overall water splitting, J. Colloid Interface Sci. 606 (2022) 873–883, https://doi.org/10.1016/j.jcis.2021.08.020.
[56] J. Tang, X. Jiang, L. Tang, Y. Li, Q. Zheng, Y. Huo, et al., Self-supported wire-in-plate NiFeS/CoS nanohybrids with a hierarchical structure for efficient overall water splitting, Dalton Trans. 50 (2021) 5921–5930, https://doi.org/10.1039/d1dt00319d.
[57] S. Duan, Z. Liu, H. Zhuo, T. Wang, J. Liu, L. Wang, et al., Hydrochloric acid corrosion induced bifunctional free-standing NiFe hydroxide nanosheets towards high-performance alkaline seawater splitting, Nanoscale 12 (2020) 21743–21749, https://doi.org/10.1039/D0NR05458E.
[58] K. Jiang, W. Liu, W. Lai, M. Wang, Q. Li, Z. Wang, et al., NiFe layered double hydroxide/FeOOH heterostructure nanosheets as an efficient and durable bifunctional electrocatalyst for overall seawater splitting, Inorg. Chem. 60 (2021) 17371–17378, https://doi.org/10.1021/acs.inorgchem.1c02903.

[59] G. Liu, Y. Xu, T. Yang, L. Jiang, Recent advances in electrocatalysts for seawater splitting, Nano Mater. Sci. (2020), https://doi.org/10.1016/j.nanoms.2020.12.003. S2589965120300659.
[60] K. Zeng, D. Zhang, Recent progress in alkaline water electrolysis for hydrogen production and applications, Prog Energy Combust. Sci. 36 (2010) 307–326, https://doi.org/10.1016/j.pecs.2009.11.002.
[61] S. Jiang, H. Suo, T. Zhang, C. Liao, Y. Wang, Q. Zhao, et al., Recent advances in seawater electrolysis, Catalysts 12 (2022) 123, https://doi.org/10.3390/catal12020123.
[62] K.N. Knust, D. Hlushkou, U. Tallarek, R.M. Crooks, Electrochemical desalination for a sustainable water future, Chemelectrochem 1 (2014) 850–857, https://doi.org/10.1002/celc.201300236.
[63] L. Zhuang, S. Li, J. Li, K. Wang, Z. Guan, C. Liang, et al., Recent advances on hydrogen evolution and oxygen evolution catalysts for direct seawater splitting, Coatings 12 (2022) 659, https://doi.org/10.3390/coatings12050659.
[64] H. Zhang, Y. Luo, P.K. Chu, Q. Liu, X. Liu, S. Zhang, et al., Recent advances in non-noble metal-based bifunctional electrocatalysts for overall seawater splitting, J. Alloys Compd. 922 (2022), 166113, https://doi.org/10.1016/j.jallcom.2022.166113.
[65] Y. Kuang, M.J. Kenney, Y. Meng, W.-H. Hung, Y. Liu, J.E. Huang, et al., Solar-driven, highly sustained splitting of seawater into hydrogen and oxygen fuels, Proc. Natl. Acad. Sci. USA 116 (2019) 6624–6629, https://doi.org/10.1073/pnas.1900556116.
[66] S. Dresp, F. Dionigi, M. Klingenhof, P. Strasser, Direct electrolytic splitting of seawater: opportunities and challenges, ACS Energy Lett. 4 (2019) 933–942, https://doi.org/10.1021/acsenergylett.9b00220.
[67] J. Mohammed-Ibrahim, H. Moussab, Recent advances on hydrogen production through seawater electrolysis, Mater. Sci. Energy Technol. 3 (2020) 780–807, https://doi.org/10.1016/j.mset.2020.09.005.
[68] R. d'Amore-Domenech, T.J. Leo, Sustainable hydrogen production from offshore marine renewable farms: techno-energetic insight on seawater electrolysis technologies, ACS Sustain. Chem. Eng. 7 (2019) 8006–8022, https://doi.org/10.1021/acssuschemeng.8b06779.
[69] S. Dresp, F. Dionigi, S. Loos, J. Ferreira de Araujo, C. Spöri, M. Gliech, et al., Direct electrolytic splitting of seawater: activity, selectivity, degradation, and recovery studied from the molecular catalyst structure to the electrolyzer cell level, Adv Energy Mater. 8 (2018), 1800338, https://doi.org/10.1002/aenm.201800338.
[70] J. Juodkazytė, B. Šebeka, I. Savickaja, M. Petrulevičienė, S. Butkutė, V. Jasulaitienė, et al., Electrolytic splitting of saline water: durable nickel oxide anode for selective oxygen evolution, Int. J. Hydrogen Energy 44 (2019) 5929–5939, https://doi.org/10.1016/j.ijhydene.2019.01.120.
[71] F. Ganci, B. Buccheri, B. Patella, E. Cannata, G. Aiello, P. Mandin, et al., Electrodeposited nickel-zinc alloy nanostructured electrodes for alkaline electrolyzer, Int. J. Hydrogen Energy (2021), https://doi.org/10.1016/j.ijhydene.2021.09.221. S0360319921038362.
[72] A.J. Bard, L.R. Faulkner, Electrochemical Methods: Fundamentals and Applications, 2nd ed., Wiley, New York, 2001.
[73] F. Schröper, D. Brüggemann, Y. Mourzina, B. Wolfrum, A. Offenhäusser, D. Mayer, Analyzing the electroactive surface of gold nanopillars by electrochemical methods for electrode miniaturization, Electrochim. Acta 53 (2008) 6265–6272, https://doi.org/10.1016/j.electacta.2008.03.068.
[74] K.I. Siwek, S. Eugénio, D.M.F. Santos, M.T. Silva, M.F. Montemor, 3D nickel foams with controlled morphologies for hydrogen evolution reaction in highly alkaline media, Int. J. Hydrogen Energy 44 (2019) 1701–1709, https://doi.org/10.1016/j.ijhydene.2018.11.070.
[75] J. Choi, A. Nkhama, A. Kumar, S.R. Mishra, F. Perez, R.K. Gupta, A facile preparation of sulfur doped nickel-iron nanostructures with improved HER and supercapacitor performance, Int. J. Hydrogen Energy 47 (2022) 7511–7521, https://doi.org/10.1016/j.ijhydene.2021.12.117.
[76] F. Dionigi, T. Reier, Z. Pawolek, M. Gliech, P. Strasser, Design criteria, operating conditions, and nickel-iron hydroxide catalyst materials for selective seawater electrolysis, ChemSusChem 9 (2016) 962–972, https://doi.org/10.1002/cssc.201501581.
[77] Y. Wu, C. Sun, H. Wang, S. Ji, B.G. Pollet, J. Lu, et al., Ni2P nanoparticles-inserted NiFeP nanosheets with rich interfaces as efficient catalysts for the oxygen evolution reaction, J. Alloys Compd. 903 (2022), 163855, https://doi.org/10.1016/j.jallcom.2022.163855.
[78] L. Negahdar, F. Zeng, S. Palkovits, C. Broicher, R. Palkovits, Mechanistic aspects of the electrocatalytic oxygen evolution reaction over Ni−Co oxides, ChemElectroChem 6 (2019) 5588–5595, https://doi.org/10.1002/celc.201901265.
[79] V.D. Silva, T.A. Simões, J.P.F. Grilo, E.S. Medeiros, D.A. Macedo, Impact of the NiO nanostructure morphology on the oxygen evolution reaction catalysis, J. Mater. Sci. 55 (2020) 6648–6659, https://doi.org/10.1007/s10853-020-04481-1.
[80] J. Kibsgaard, I. Chorkendorff, Considerations for the scaling-up of water splitting catalysts, Nat. Energy 4 (2019) 430–433, https://doi.org/10.1038/s41560-019-0407-1.
[81] S. Dresp, T. Ngo Thanh, M. Klingenhof, S. Brückner, P. Hauke, P. Strasser, Efficient direct seawater electrolysers using selective alkaline NiFe-LDH as OER catalyst in asymmetric electrolyte feeds, Energy Environ. Sci. 13 (2020) 1725–1729, https://doi.org/10.1039/D0EE01125H.
[82] N. Kishimoto, State of the art of UV/chlorine advanced oxidation processes: their mechanism, byproducts formation, process variation, and applications, J. WaterEnviron. Technol. 17 (2019) 302–335, https://doi.org/10.2965/jwet.19-021.
[83] H. Yang, M. Driess, P.W. Menezes, Self-supported electrocatalysts for practical water electrolysis, Adv. Energy Mater. 11 (2021), 2102074, https://doi.org/10.1002/aenm.202102074.
[84] O. Dragos, H. Chiriac, N. Lupu, M. Grigoras, I. Tabakovic, Anomalous codeposition of *fcc* NiFe nanowires with 5-55% Fe and their morphology, crystal structure and magnetic properties, J. Electrochem. Soc. 163 (2016) D83–D94, https://doi.org/10.1149/2.0771603jes.
[85] P. Jing, M. Liu, Y. Pu, Y. Cui, Z. Wang, J. Wang, et al., Dependence of phase configurations, microstructures and magnetic properties of iron-nickel (Fe-Ni) alloy nanoribbons on deoxidization temperature in hydrogen, Sci. Rep. 6 (2016) 37701, https://doi.org/10.1038/srep37701.
[86] Y. Gao, Z. Zhao, H. Jia, X. Yang, X. Lei, X. Kong, et al., Partially reduced Ni^{2+}, Fe^{3+}-layered double hydroxide for ethanol electrocatalysis, J. Mater. Sci. 54 (2019) 14515–14523, https://doi.org/10.1007/s10853-019-03964-0.
[87] F. Maurer, J. Brötz, S. Karim, M.E.T. Molares, C. Trautmann, H. Fuess, Preferred growth orientation of metallic fcc nanowires under direct and alternating electrodeposition conditions, Nanotechnology 18 (2007), 135709, https://doi.org/10.1088/0957-4484/18/13/135709.